Design of a Novel Multicylinder Stirling Engine

Steven Chatterton[1]
Mem. ASME
Department of Mechanical Engineering,
Politecnico di Milano,
Via G. La Masa 1,
Milano 20156, Italy
e-mail: steven.chatterton@polimi.it

Paolo Pennacchi
Mem. ASME
Department of Mechanical Engineering,
Politecnico di Milano,
Via G. La Masa 1,
Milano 20156, Italy

Stirling engines are machines based on a simple working principle and are well known for their theoretical high thermal efficiency. Technical drawbacks related to the high temperatures required for achieving high values of thermal efficiency and output power have limited their spread to low-power applications. Stirling engines can operate with almost any source of heat. For this reason, these engines are currently installed in applications with renewable energy sources for combined heat and power generation (CHP), where the mechanical output power is usually converted into electrical power. The paper is focused on the design and analysis of a novel mechanical configuration with a higher number of cylinders than current commercial solutions. The performances of several multicylinder configurations are evaluated via numerical simulations, taking into account the dynamics of the mechanism and the thermal aspects of the cycle. Finally, a prototype of the main mechanism, which allows the number of cylinders to be increased, is introduced and briefly described. [DOI: 10.1115/1.4029642]

Keywords: stirling engine, multicylinder configuration, dynamic model, planetary mechanism

Introduction

Stirling engines operate a closed regenerative thermodynamic cycle with cyclic compression and expansion of the working gas at different temperature levels provided by two thermal sources [1], resulting in a net conversion of heat to work. The possibility of operating with almost any heat source has increased the installation of Stirling engines in the renewable energy field, typically in small applications for CHP generation, where a small combustion engine is coupled with an electrical generator for the production of electrical and thermal power.

Since its invention in 1816, several mechanisms have been developed to convert the displacement of pistons in the compression and expansion chambers into angular or linear displacement of the output shaft. By considering the general arrangement of the engine, three different types are defined [2], i.e., α-, β-, and γ-types.

Currently, from a kinematic point of view, two main groups of engines could be identified: *free-piston* and *kinematic drive machines*. Free-piston devices are single-cylinder engines without a direct connection of the electrical generator to the power piston [3]. Commercial units of this engine for microcogeneration use Helium as the working fluid and are able to generate up to 1 kW of electrical power and 4–5 kW of thermal power. The second group includes conventional machines composed of mechanical parts, such as cranks, connecting rods, pistons, etc. [2]. In this last group, several mechanisms have been proposed and developed for the connection of the power pistons to the main shaft of the electrical generator: the slider-crank, Scotch yoke, Ross yoke, swash plate, wobble yoke, rhombic drive, Bell crank, and X-yoke. Four-cylinder engine equipped with the wobble yoke mechanism is the most widely developed and available model on the market [4–7].

Common drawbacks of the free-piston and four-cylinder models are due to the high temperature of the thermal source required for high thermal efficiency. Sealing and material fatigue are critical from the mechanical point of view.

Some attempts to improve the Stirling engine design, from a mechanical point of view, are available in the literature; the reduction of the overall dimensions is discussed in Ref. [8]. A lever-controlled displacer driving mechanism with a single-cylinder is proposed in Refs. [9] and [10]. A regenerative displacer is studied in Ref. [11], while the surface treatment of the displacer with a zirconium coating for similar purposes is discussed in Ref. [12]. The dynamic stability of the free-piston type is discussed in Ref. [13] from a control point of view. The optimization of the phase angle, considering the effect of the overlapping volume between compression and expansion spaces with a rhombic drive, is discussed in Ref. [14].

The aim of this paper is to investigate several multicylinder configurations to improve the performances of Stirling engines in the kinematic drive group [15]. Thermal and mechanical problems related to the high temperature of the unit are not considered in the paper. The increase in the total net power and the overall efficiency is the direct consequence of the increase in the number of cylinders in the same engine. Furthermore, multicylinder configurations lead to a reduction in torque and speed oscillations over a revolution of the shaft of the electrical generator as well as to the optimal selection of the phase angle between cylinders and cycles. The performance of each configuration is evaluated using numerical simulation and a suitable model of the system proposed by the authors. In particular, the models of the thermodynamic cycle and the mechanical part have been developed and fully described in the paper.

A novel solution, based on a planetary mechanism and a preliminary optimization of the geometrical parameters of the kinematic scheme, is introduced.

Model of the Thermodynamic Cycle

The ideal Stirling thermodynamic cycle is composed of four phases: (i) *isothermal compression*, where the temperature remains constant (1–2 in Fig. 1); (ii) *isochoric heating*, where the volume remains constant (2–3 in Fig. 1); (iii) *isothermal expansion* (3–4 in Fig. 1); and (iv) *isochoric cooling* (4-1 in Fig. 1).

The efficiency of the ideal Stirling cycle corresponds to the Carnot cycle and depends only on the heating and cooling temperature of the two thermal sources. However, real Stirling cycles are quite different from ideal ones; isochoric transformations are

[1]Corresponding author.

Contributed by the Mechanisms and Robotics Committee of ASME for publication in the Journal of Mechanical Design. Manuscript received May 6, 2014; final manuscript received January 6, 2015; published online February 16, 2015. Assoc. Editor: Ettore Pennestri.

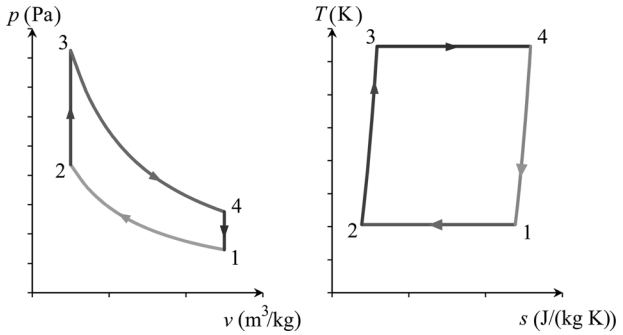

Fig. 1 Thermodynamic Stirling cycle

actually realized by the continuous displacement of pistons whereas adiabatic transformations occur instead of isothermal ones.

A simple model of the thermodynamic cycle is reported in Fig. 2. It consists of five consecutive cells serially connected, corresponding to the physical components of the system:

(1) The compression space at temperature T_c, where an adiabatic transformation occurs.
(2) The cooler, ideally held at constant temperature T_k.
(3) The regenerator, where the temperature T_r is supposed to change linearly from the lower temperature T_k of the cooler to the higher temperature T_h of the heater; a constant equivalent temperature is assumed [8,16].

$$T_r = (T_h - T_k)/\ln(T_h - T_k) \tag{1}$$

The regenerator is an additional component, generally a stainless steel mesh, placed between the heater and the cooler exchangers and able to increase the cycle efficiency [17].

(1) The heater ideally held at constant temperature T_h.
(2) The expansion space at temperature T_e, where an adiabatic transformation occurs.

The temperature in the compression and expansion cells is not constant but varies over a complete cycle due to the assumption of adiabatic transformations.

In this ideal model, the heat exchangers are perfectly effective: there is no leakage, the total mass M of the gas is constant and there is no pressure drop between cells.

The set of equations of the thermodynamic model is obtained for each cell, yielding the energy equation

$$c_p\left(T_{(j-1)\to j}\dot{m}_{(j-1)\to j} - T_{j\to(j+1)}\dot{m}_{j\to(j+1)}\right) + \frac{d}{dt}Q_j = \frac{d}{dt}W_j + c_v\frac{d}{dt}\left(m_jT_j\right) \tag{2}$$

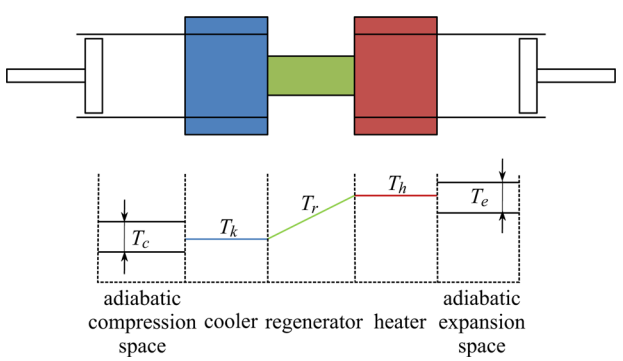

Fig. 2 Model of the thermodynamic cycle and temperature profile in the cells

where the subscript $j \in \{c,k,r,h,e\}$ indicates the jth cell with c as the compression space, k as the cooler, r as the regenerator, h as the heater and e as the expansion space; c_p and c_v are the specific heat of the gas at constant pressure and constant volume, respectively; $\dot{m}_{(j-1)\to j}$ and $\dot{m}_{j\to(j+1)}$ are the inlet and outlet mass flow in the cell characterized by the temperatures $T_{(j-1)\to j}$ and $T_{j\to(j+1)}$, respectively. Additionally, m_j and T_j are the mass and the temperature of the cell, Q_j indicates the heat transfer into the cell, and W_j indicates the work performed on the surroundings.

Considering an ideal working gas and the constancy of the total mass of the gas in the machine, a set of differential equations can be obtained [16]

— *Fluid masses and mass flows in the cells*

$$\begin{aligned} M &= \sum_j m_j \\ m_j &= pV_j/(RT_j) \\ \dot{m}_c &= \left(p\dot{V}_c + \dot{p}V_c/\gamma\right)/(RT_{c\to k}) \\ \dot{m}_k &= m_k\dot{p}/p \\ \dot{m}_r &= m_r\dot{p}/p \\ \dot{m}_h &= m_h\dot{p}/p \\ \dot{m}_e &= \left(p\dot{V}_e + \dot{p}V_e/\gamma\right)/(RT_{h\to e}) \end{aligned} \tag{3}$$

— *Mass flows between cells*

$$\begin{aligned} \dot{m}_{c\to k} &= -\dot{m}_c \\ \dot{m}_{k\to r} &= \dot{m}_{c\to k} - \dot{m}_k \\ \dot{m}_{r\to h} &= \dot{m}_{h\to e} + \dot{m}_h \\ \dot{m}_{h\to e} &= \dot{m}_e \end{aligned} \tag{4}$$

— *Temperatures and temperature derivatives*

$$\begin{aligned} \dot{T}_c &= T_c\left(\dot{p}/p + \dot{V}_c/V_c - \dot{m}_c/m_c\right) \\ T_{c\to k} &= \begin{cases} T_c & \text{if} \quad \dot{m}_{c\to k} > 0 \\ T_k & \text{if} \quad \dot{m}_{c\to k} < 0 \end{cases} \\ T_{h\to e} &= \begin{cases} T_h & \text{if} \quad \dot{m}_{h\to e} > 0 \\ T_e & \text{if} \quad \dot{m}_{h\to e} < 0 \end{cases} \\ \dot{T}_e &= T_e\left(\dot{p}/p + \dot{V}_e/V_e - \dot{m}_e/m_e\right) \end{aligned} \tag{5}$$

— *Pressure and pressure derivative*

$$\begin{aligned} p &= \frac{MR}{\sum_j V_j/T_j} \\ \dot{p} &= \frac{-\gamma p\left(\dot{V}_c/T_{c\to k} + \dot{V}_e/T_{h\to e}\right)}{V_c/T_{c\to k} + V_e/T_{h\to e} + \gamma(V_k/T_k + V_r/T_r + V_h/T_h)} \end{aligned} \tag{6}$$

— *Heat transfer and total work*

$$\begin{aligned} \dot{Q}_c &= 0 \\ \dot{Q}_k &= V_k\dot{p}c_v/R - c_p(T_{c\to k}\dot{m}_{c\to k} - T_k\dot{m}_{k\to r}) \\ \dot{Q}_r &= V_r\dot{p}c_v/R - c_p(T_k\dot{m}_{k\to r} - T_h\dot{m}_{r\to h}) \\ \dot{Q}_h &= V_h\dot{p}c_v/R - c_p(T_h\dot{m}_{r\to h} - T_{h\to e}\dot{m}_{h\to e}) \\ \dot{Q}_e &= 0 \\ \dot{W} &= p\left(\dot{V}_c + \dot{V}_e\right) \end{aligned} \tag{7}$$

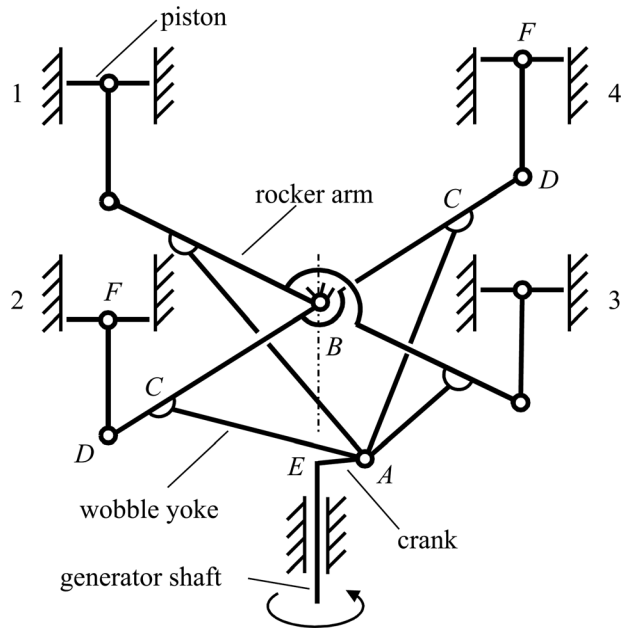

Fig. 3 Four-cylinder configuration with wobble yoke mechanism

where V_j is the volume of the jth cell, R is the individual gas constant and $\gamma = c_p/c_v$.

Multicylinder Configurations

The main limitation of commercial Stirling engines in multicylinder configurations is the number of the cylinders connected to the same shaft of the electrical generator. Stirling machines based on the wobble yoke mechanism have a maximum of four cylinders and, therefore, four thermodynamic cycles. The relative phase between two consecutive cycles is equal to the geometrical phase angle between two consecutive cylinders.

This limitation means that the $(n+1)$th cycle follows the nth cycle and the $(n+1)$th cylinder follows the nth cylinder. For example, the thermodynamic cycle #1 is given by the connection of the compression chamber of cylinder #1 to the expansion chamber of cylinder #2.

Furthermore, the wobble yoke mechanism of a commercial four-cylinder engine has two rocker arms sharing the same revolute joint in B connected to the fixed reference system (Fig. 3), where two opposite pistons are connected by the same rocker arm (e.g., pistons 1 and 3 in Fig. 3). In Fig. 3, the two rocker arms are connected to the crank of the shaft of the electrical generator by several wobble rods (e.g., rods AC in Fig. 3).

The adoption of more than four cylinders needs a different mechanism that is able to avoid the collisions between the wobble rods of the mechanism. The additional cylinders to the basic four-cylinder engine allow the total net power to be increased and the torque and rotational speed oscillations to be reduced during the revolution. Moreover, the phase angle between consecutive thermodynamic cycles can be optimized and different from the geometrical phase angle between two consecutive cylinders. For example, in a multicylinder configuration, thermodynamic cycle #1 could be given by the connection of the compression chamber of cylinder #1 to the expansion chamber of cylinder #3.

Several cycle connections are possible for multicylinder configurations as shown in Fig. 4 for several cylinders varying from 5 to 8. The number of thermodynamic cycles is equal to the number of cylinders and the $(n+1)$th cylinder follows the nth cylinder.

In Fig. 4, the lines represent the connections of the thermodynamic cycles among the cylinders, which are represented by dots. The notation $k(n+w)$ used in Fig. 4 means that, for an engine with k cylinders, the nth thermodynamic cycle is given by the connection of the compression space of the nth cylinder and the expansion space of the $(n+w)$th cylinder. The number below each scheme represents the phase angle between two consecutive cycles. The configurations $k(n+1)$ represent engines with cycles connected in series. For example, commercial four-cylinder wobble yoke engines have a $4(n+1)$configuration. The star configuration $6(n+2)$ represents a double system with two serial $3(n+1)$configurations working in parallel and the $8(n+2)$ configuration represents two $4(n+1)$ systems.

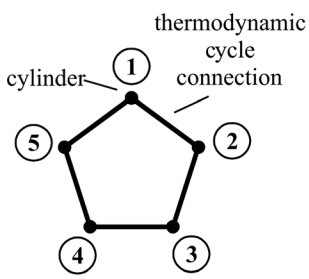

Cylinders	$k=5$	$k=6$	$k=7$	$k=8$
Conn. $k(n+1)$	(72°)	(60°)	(~51.4°)	(45°)
Conn. $k(n+2)$	(144°)	(120°)	(~102.8°)	(90°)
Conn. $k(n+3)$			(~154.2°)	(135°)

Fig. 4 Multicylinder configurations with different cycle connections

Novel Kinematic Scheme

As introduced before, starting from the four-cylinder configuration, the increase in the number of cylinders requires some modifications to the basic kinematic scheme with the wobble yoke of Fig. 3. In particular, it is not physically possible to add another rocker arm to this scheme due to some design limitations. In this case, additional rocker arms only allow for configurations with even cylinder numbers. To avoid this constraint, a solution is the adoption of different mechanisms, such as swash-plates or spatial cams. The aim of the authors is:

- To propose and prove the effectiveness of an unusual kinematic scheme.
- To maintain the well known slider-crank mechanism for the displacement of the pistons.

Some modifications are then introduced in the kinematic scheme of commercial four-cylinder Stirling engines equipped with wobble yoke mechanisms.

The first is the use of independent rocker arms for each cylinder, allowing for configurations with an odd number of cylinders. The second is the adoption of a planetary mechanism for the connection of the wobble rods (*AC* in Fig. 3) to the crankshaft of the electrical generator. This second modification allows the number of cylinders to be increased, and the collision of wobble rods during a revolution to be avoided.

The final kinematic scheme for a five-cylinder configuration is shown in Fig. 5. The rocker arm *GD* in Fig. 5 is connected to the fixed frame via the revolute joint *G* at a distance $\overline{BG}$ from the revolution axis of the shaft of the electrical generator. The distance $\overline{BG}$ is set to be equal to the distance $\overline{HA}$. In this way, the basic scheme of Fig. 3 is maintained, and it is only translated from the axis of the shaft of the electrical generator by the distance $\overline{BG}$. The motion of the planetary disk that holds the revolute joint *A* of the wobble rods *AC* is a simple translation at null angular speed around the revolution axis. This condition is realized via a suitable planetary mechanism, such as a timing belt coupled with two identical timing pulleys or a gear train (see Fig. 6). In the following discussion, the solution based on planetary gears will be described.

Each piston of the scheme in Fig. 5 is connected to the shaft of the electrical generator through two mechanisms placed in series. The principal one is the planetary mechanism, which links the angular rotation α of the shaft of the electrical generator to the angular rotation ϕ_n of the *n*th rocker arm. The secondary one is a slider-crank mechanism that connects the rocker arm angular rotation ϕ_n to the piston displacement $y_{p,n}$ (Fig. 7).

The kinematic equation of the planetary mechanism is given by

$$A \sin\phi_n + B_n \cos\phi_n = D_n \tag{8}$$

where

$$\begin{aligned} A &= 2\overline{BE}\cdot\overline{GC} \\ B_n &= 2\overline{GC}\cdot\left[\overline{BG}-\overline{HA}-\overline{EH}\cdot\cos(\alpha-\delta_n)\right] \\ D_n &= \overline{AC}^2-\overline{EH}^2-\overline{HA}^2-\overline{BG}^2-\overline{GC}^2-\overline{BE}^2 \\ &\quad +2\overline{HA}\cdot\overline{BG}-2\overline{EH}\cdot\left(\overline{HA}-\overline{BG}\right)\cdot\cos(\alpha-\delta_n) \end{aligned} \tag{9}$$

and $\delta_n = 2\pi/N$ is the geometrical phase between two consecutive cylinders.

The solution to Eq. (9) allows the angular rotation ϕ_n of the *n*th rocker arm to be obtained as a function of the angular rotation α of the shaft of the electrical generator

$$\phi_n(\alpha) = 2tan^{-1}\left(\frac{A-\sqrt{A^2+B_n^2(\alpha)-D_n^2(\alpha)}}{B_n(\alpha)+D_n(\alpha)}\right) \tag{10}$$

The angular velocity and the acceleration of the *n*th rocker arm are reported for completeness in Eq. (11)

$$\begin{aligned} \dot{\phi}_n &= \frac{\dot{D}_n-\dot{B}_n\cos\phi_n}{A\cos\phi_n-B_n\sin\phi_n} \\ \ddot{\phi}_n &= \frac{\ddot{D}_n-\ddot{B}_n\cos\phi_n+\left[2\dot{B}_n\sin\phi_n+\dot{\phi}_n(A\sin\phi_n+B_n\cos\phi_n)\right]\dot{\phi}_n}{A\cos\phi_n-B_n\sin\phi_n} \\ \dot{B}_n &= 2\dot{\alpha}\overline{EH}\cdot\overline{GC}\sin(\alpha-\delta_n) \\ \dot{D}_n &= 2\dot{\alpha}\overline{EH}\left(\overline{HA}-\overline{BG}\right)\sin(\alpha-\delta_n) \\ \ddot{B}_n &= 2\overline{EH}\cdot\overline{GC}\left[\ddot{\alpha}\sin(\alpha-\delta_n)+\dot{\alpha}^2\cos(\alpha-\delta_n)\right] \\ \ddot{D}_n &= 2\overline{EH}\left(\overline{HA}-\overline{BG}\right)\left[\ddot{\alpha}\sin(\alpha-\delta_n)+\dot{\alpha}^2\cos(\alpha-\delta_n)\right] \end{aligned} \tag{11}$$

With reference to Fig. 7, the displacement $y_{p,n}$ of the piston as function of the angular rotation ϕ_n of the rocker arm in the secondary mechanism is given by

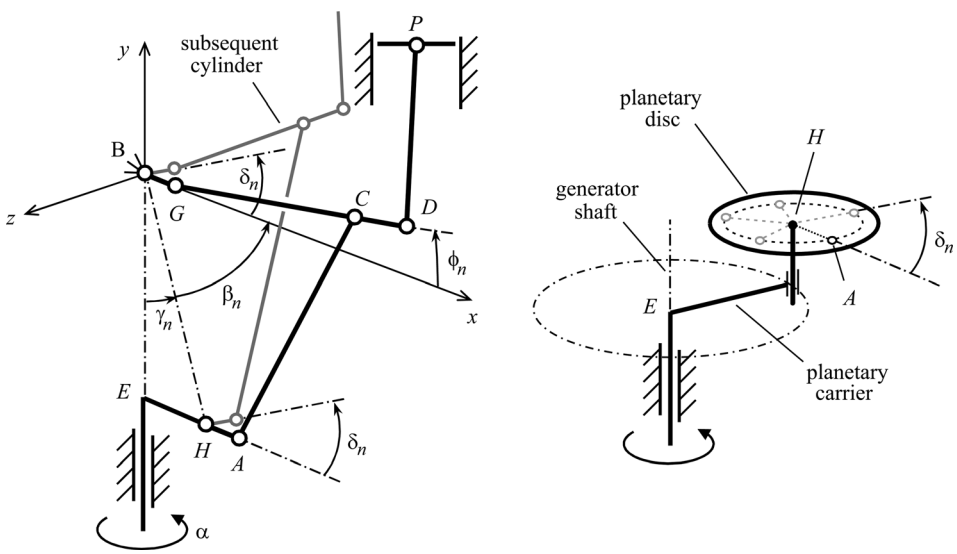

Fig. 5 Kinematic scheme of the planetary mechanism

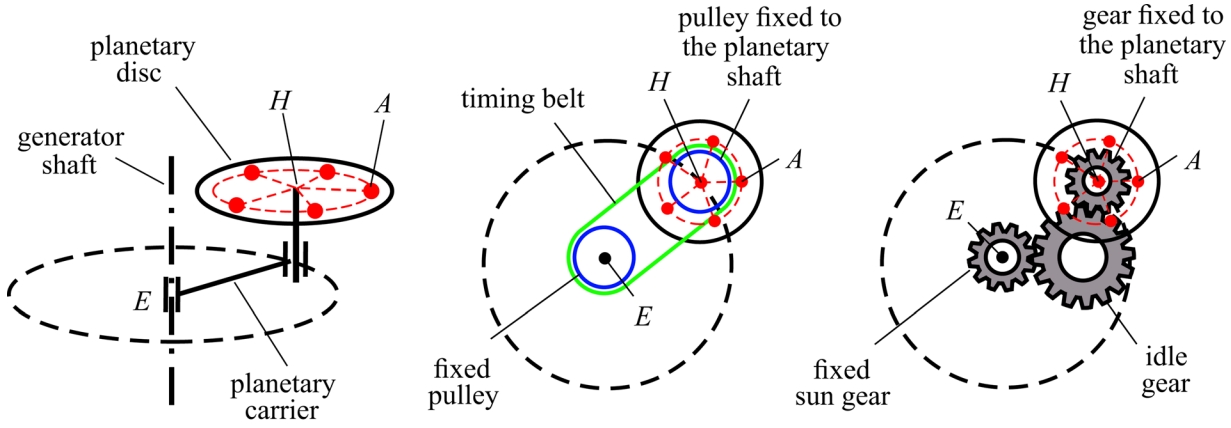

Fig. 6 Planetary mechanism and design solutions: (*b*) timing belt and pulleys or (*c*) gears

$$y_{p,n}(\phi_n) = \overline{GD}\sin\phi_n + \overline{DP}\sin\epsilon_n$$
$$\epsilon_n = \arccos\left(\frac{\overline{KF}}{\overline{DP}} - \frac{\overline{GD}}{\overline{DP}}\cos\phi_n\right) \tag{12}$$

The piston velocity and acceleration follows:

$$\dot{y}_{p,n} = \overline{BD}\dot{\phi}_n\cos\phi_n + \overline{DP}\dot{\epsilon}_n\cos\epsilon_n$$
$$\ddot{y}_{p,n} = \overline{BD}(\ddot{\phi}_n\cos\phi_n - \dot{\phi}_n^2\sin\phi) + \overline{DP}(\epsilon_n\cos\epsilon_n - \dot{\epsilon}_n^2\sin\epsilon_n)$$
$$\dot{\epsilon}_n = -\frac{\overline{BD}}{\overline{DP}}\frac{\sin\phi}{\sin\epsilon}\dot{\phi}_n$$
$$\epsilon_n = -\left[\frac{\overline{BD}}{\overline{DP}\sin\epsilon_n}\left(\dot{\phi}_n^2\cos\phi_n + \ddot{\phi}_n\sin\phi_n\right) + \frac{\dot{\epsilon}_n^2}{\tan\epsilon_n}\right] \tag{13}$$

Prototype Design. A 3D model of the proposed kinematic scheme for a five-cylinder configuration is shown in Fig. 8 for two different configurations of the rocker arms. The solution of Fig. 8(*b*)) allows the reduction of the overall dimensions of the system.

Some pictures of a prototype of the proposed mechanism are shown in Fig. 9. In particular, due to the high cost required for an entire engine, a four-cylinder commercial Stirling unit has been-modified, and the wobble yoke mechanism has been replaced with the proposed kinematic scheme adapted for a $4(n+1)$-cylinder configuration. The benefits of configurations with more cylinders will be explained via simulations.

Dynamic Model

The forces involved in the functioning of the nth cylinder are shown in Fig. 10 where:

- J_{DP} is the mass moment of inertia of the connecting rod with mass m_{DP} with respect to joint P.
- J_{GD} is the mass moment of inertia of the rocker arm with mass m_{GD} with respect to joint D.
- J_{EH} the mass moment of inertia of the planetary carrier, including the inertia of the electrical generator.
- m_{HA} represents the sum of the masses of the planetary gear and its shaft.
- J_{I} indicates the mass moment of inertia of the idle gear with mass m_{I}.
- m_{AC} is the mass of the wobble rod.
- m_{p} is the mass of the piston and the crosshead.

The differential equation of the mechanical model could be easily obtained for the nth cylinder configuration by applying the kinetic energy theorem in terms of the power balance of the entire mechanism

$$\sum P = \frac{d}{dt}T \tag{14}$$

where the left-hand term represents the sum of mechanical power due to active forces (gravity effect is neglected) and the right-hand term is the time derivative of the kinetic energy T of the entire system, resulting in

$$\sum_{n=1}^{N}\left[(F_{\mathrm{comp},n} - F_{\mathrm{exp},n})\dot{y}_{p,n}\right] - C_{\mathrm{gen}}\dot{\alpha} = \left(J_{EH} + \left(\frac{Z_E}{Z_{\mathrm{I}}} + 1\right)^2 J_{\mathrm{I}} + \left(\frac{m_{AC}}{2} + \frac{m_I}{4} + m_{HA}\right)\overline{EH}^2\right)\ddot{\alpha}\dot{\alpha}$$
$$+ \left(m_{\mathrm{p}} + \frac{m_{DP}}{2}\right)\cdot\sum_{n=1}^{N}\left[\dot{y}_{\mathrm{p},n}\ddot{y}_{\mathrm{p},n}\right] + J_{DP}\sum_{n=1}^{N}\left[\dot{\epsilon}_n\ddot{\epsilon}_n\right] + \left(J_{GD} + \frac{m_{AC}}{2}\overline{GC}^2 + \frac{m_{DP}}{2}\overline{GD}^2\right)\cdot\sum_{n=1}^{N}\left[\dot{\phi}_n\ddot{\phi}_n\right] \tag{15}$$

where the active forces are represented by the torque C_{gen} of the electrical generator and fluid forces $F_{\mathrm{exp},n}$ and $F_{\mathrm{comp},n}$ acting on the upper and the lower surfaces of the pistons, respectively. The fluid forces $F_{\mathrm{exp},n}$ and $F_{\mathrm{comp},n}$ are given by the expansion pressure $p_{\mathrm{exp},n}$ of the fluid of the $(n+1)$th thermodynamic cycle and the compression pressure $p_{\mathrm{comp},n}$ of the nth cycle. C_{gen} is the torque of the asynchronous generator given by its characteristics curve, which can be approximated by a linear equation as a function of the rotational speed around the nominal working condition $(C_0, \dot{\alpha}_0)$. Z_{E} and Z_{I} are the numbers of teeth of the sun and idle

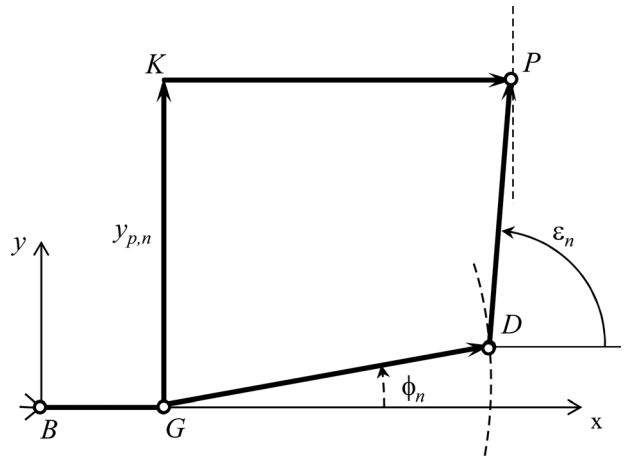

Fig. 7 Kinematic scheme of the secondary mechanism

gears, respectively (the ratio must be equal to $Z_E/Z_I = 1$). By inserting Eqs. (10)–(13) in Eq. (15), it is possible to obtain a second order differential equation with a single degree of freedom in the unknown variable α, i.e., the angular rotation of the shaft of the electrical generator.

Numerical Simulations

Equation (15) is a second order differential equation, which can be numerically integrated together with the differential equations (3)–(7) of the thermodynamic cycle.

Fig. 9 Pictures of the mechanical components of the proposed kinematic scheme for a four-cylinder configuration

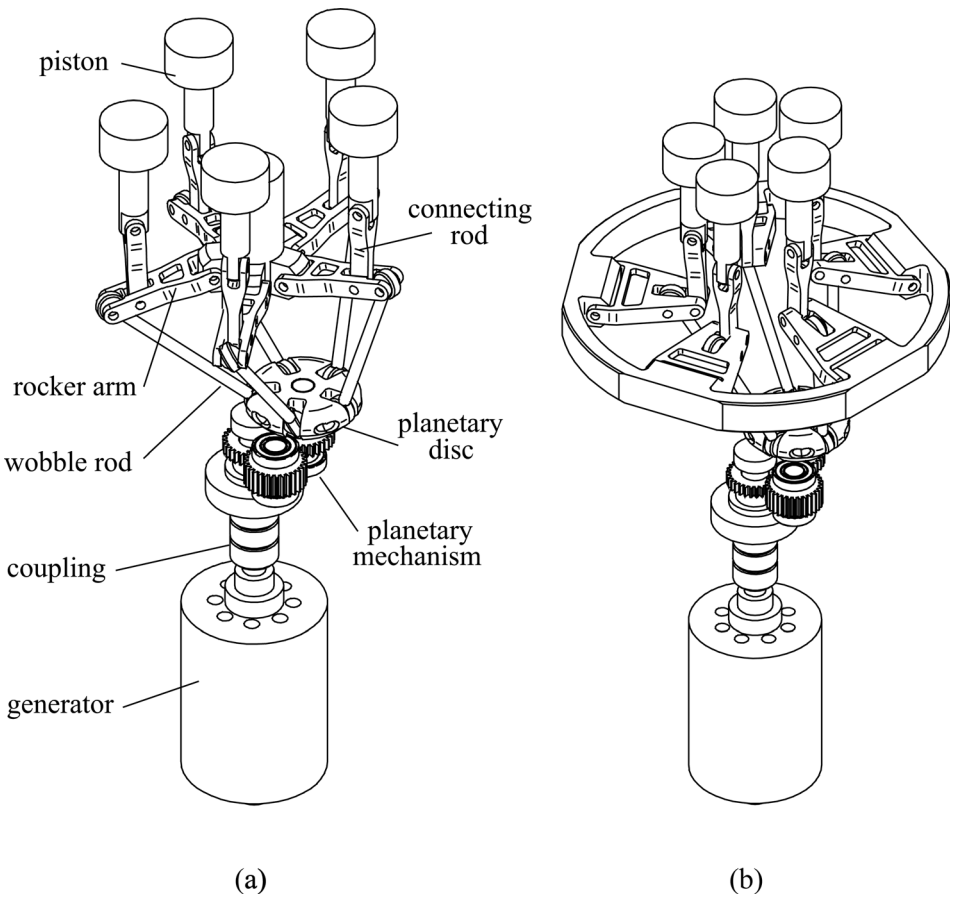

Fig. 8 Design solutions with different position of the rocker arms: (*a*) inner and (*b*) outer configurations

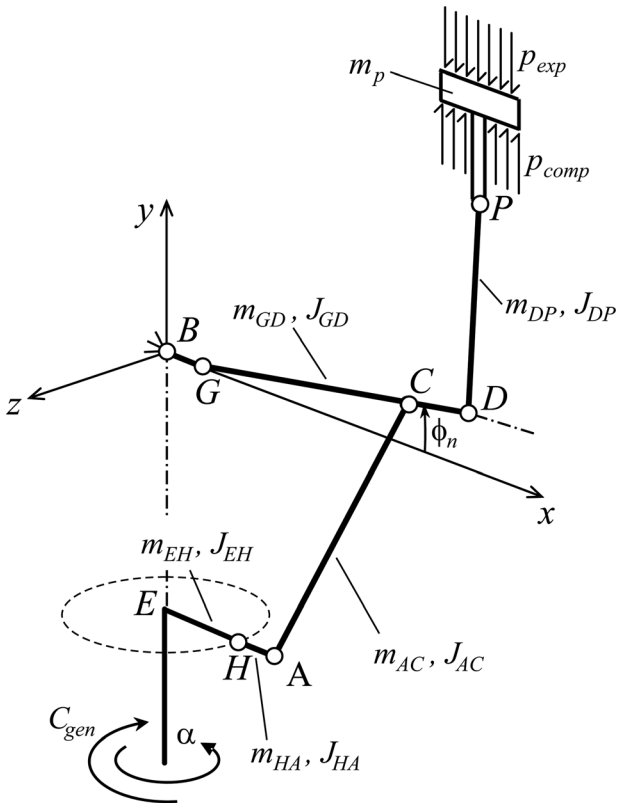

Fig. 10 Forces acting on each cylinder

Table 1 Geometrical data of the system

Piston stroke		0.020 m
Cylinder diameter	D_p	0.040 m
Stem diameter	d_s	0.022 m
Connecting rod length	DP	0.100 m
Wobble rod length	AC	0.078 m
Planetary carrier length	EH	0.009 m
Distance of joint G from the revolution axis	BG	0.011 m
Axial distance	BE	0.050 m
Rocker arm length	GD	0.050 m
Distance of joint C from joint G	GC	0.050 m
Radial position of cylinder	KP	0.050 m
Distance from the center of planetary carrier	HA	0.005 m
Moment of inertia of connecting rod	J_{DP}	6.7×10^{-5} kg m^2
Moment of inertia of rocker arm	J_{GD}	2.1×10^{-5} kg m^2
Moment of inertia of generator shaft	J_{EH}	5×10^{-3} kg m^2
Moment of inertia of idle gear	J_I	1×10^{-5} kg m^2
Mass of connecting rod	m_{DP}	0.020 kg
Mass of rocker arm	m_{GD}	0.026 kg
Mass of planetary gear and shaft	m_{HA}	0.030 kg
Mass of idle gear	m_I	0.020 kg
Mass of wobble rod	m_{AC}	0.018 kg
Mass of piston and cross-head	m_p	0.256 kg
Nominal speed	$\dot{\alpha}_0$	157 rad/s
Compression dead volume	V_{clc}	1.0×10^{-6} m^3
Compression swap volume	V_{swc}	17.3×10^{-6} m^3
Expansion dead volume	V_{cle}	3.0×10^{-6} m^3
Expansion swap volume	V_{swe}	25.1×10^{-6} m^3
Regenerator volume	V_r	10.0×10^{-6} m^3
Heater volume	V_h	6.1×10^{-6} m^3
Cooler volume	V_k	5.3×10^{-6} m^3
Mean pressure	p	1.07 MPa
Heater temperature	T_h	1073 K
Cooler temperature	T_k	323 K
Equivalent regenerator temperature	T_r	625 K
Working gas		N_2

The integration in the time domain of all of the differential equations is performed via a 4th order Runge–Kutta algorithm with 1×10^{-5} s time step. The data for the Stirling engine used in the simulations are listed in Table 1.

The generator angular speed, obtained via an integration over four shaft revolutions at nominal rotational speed of $\dot{\alpha}_0$ for a $5(n+1)$-cylinder configuration, is shown in Fig. 11. The oscillation of the solution in the first revolutions is due to the value of the initial conditions assumed at time $t = 0$, i.e., $\alpha(t = 0) = 0$ and $\dot{\alpha}(t = 0) = \dot{\alpha}_0$. The convergence of the solution to steady state requires less than one shaft revolution.

The results of the simulations (speed and torque at the generator shaft) for several configurations with different numbers of cylinders and different cycle connections, but with the same data of Table 1 (same volume and same mass of gas for each cycle), are shown in Figs. 12 and 13. The corresponding p–V diagrams for the first thermodynamic cycle of each configuration at steady state are also reported in Fig. 14.

From a general point of view, an increase in the mean value of the generator torque and a reduction of the torque oscillations can be seen in Fig. 12 for a higher number of cylinders. The same behavior is evident for the rotational speed reported in Fig. 13: the increase in the cylinder number allows the reduction of speed oscillations.

The total mean power $\bar{P}$, the mean power per cylinder $\bar{P}/N$, the mean torque $\bar{M}$ and the oscillation of the torque $\Delta\bar{M}/\bar{M}$ with respect to the mean value in the steady state, are listed in Table 2. Excluding the $6(n+2)$ and $8(n+2)$ configurations that correspond to double mechanisms, the best configurations in terms of maximum power per cylinder are the $4(n+1)$, the $5(n+1)$, and the $7(n+2)$ configurations.

The efficiency of the cycle, given by the ratio between the total work and the heat, is reported in the last column of Table 2. Considering that the efficiency of the ideal Stirling cycle is equal to $\eta = 1 - T_k/T_h = 68.4\%$ with the temperatures listed in Table 1, a small improvement in the efficiency is seen in the $5(n+1)$ and $7(n+1)$ configurations. However, the efficiency is evaluated under the hypothesis of ideal heat exchangers, an ideal regenerator and neglecting the frictional forces caused by the seals between the pistons and the cylinders.

Interesting results come from the evaluation of the joint forces. Considering the kinematic scheme in Fig. 5, points P and D are represented by cylindrical joints, points A and C by spherical joints, and point G by a revolute joint. For the sake of brevity only plots of the joint forces for points P, A, and G are shown in the paper. The joint forces for points D and P differ only by the inertial forces of connecting rod DP, whereas the joint forces for

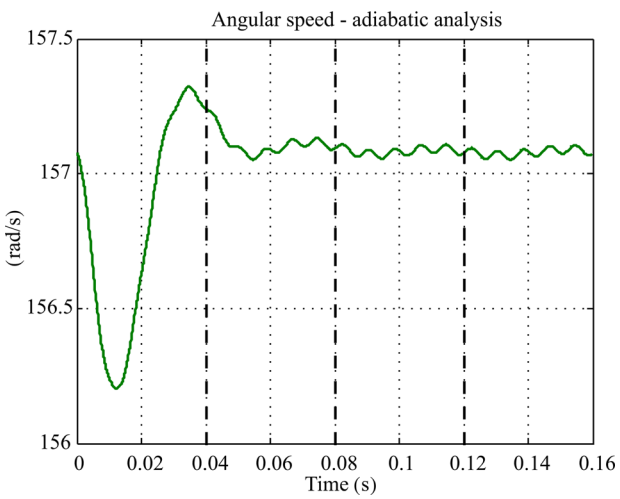

Fig. 11 Generator angular speed for the 5 (n + 1)-cylinder configuration. Vertical dashed lines represent shaft revolutions.

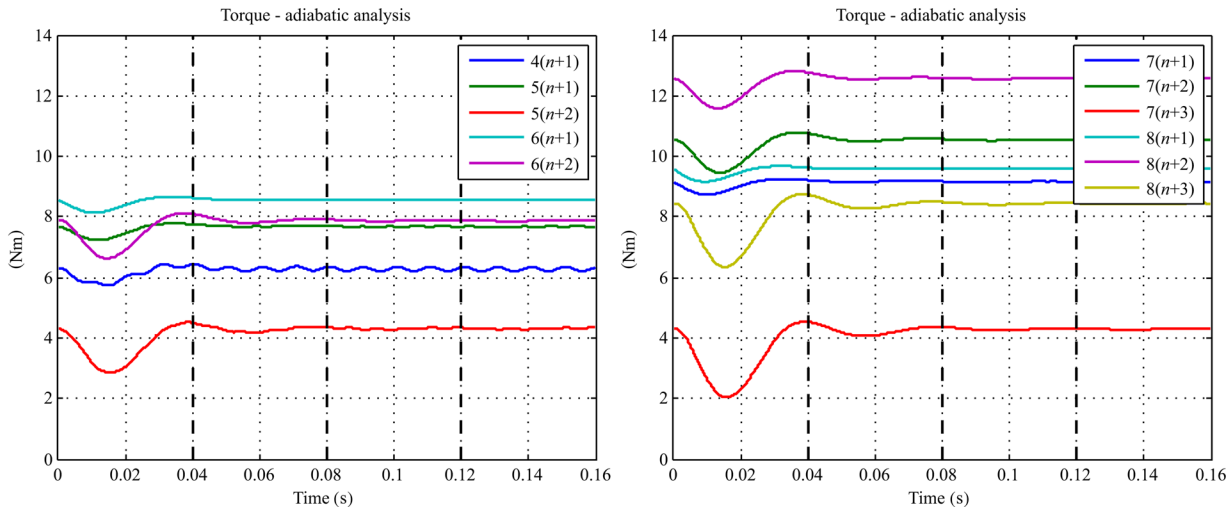

Fig. 12 Torque at the generator shaft for different cylinder configurations. Vertical dashed lines represent shaft revolutions.

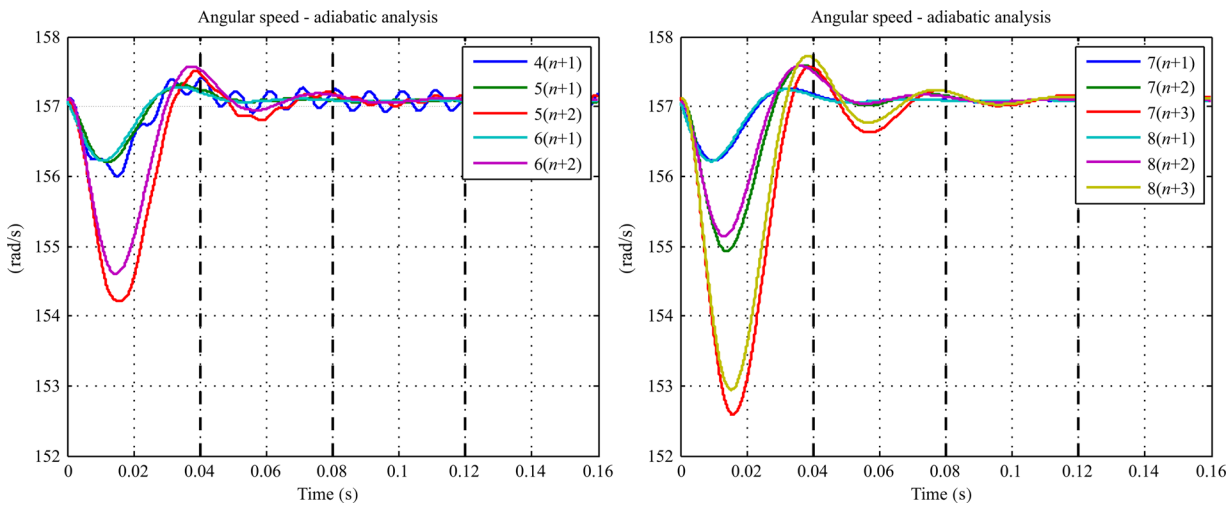

Fig. 13 Rotational speed of the generator shaft for different cylinder configurations. Vertical dashed lines represent shaft revolutions.

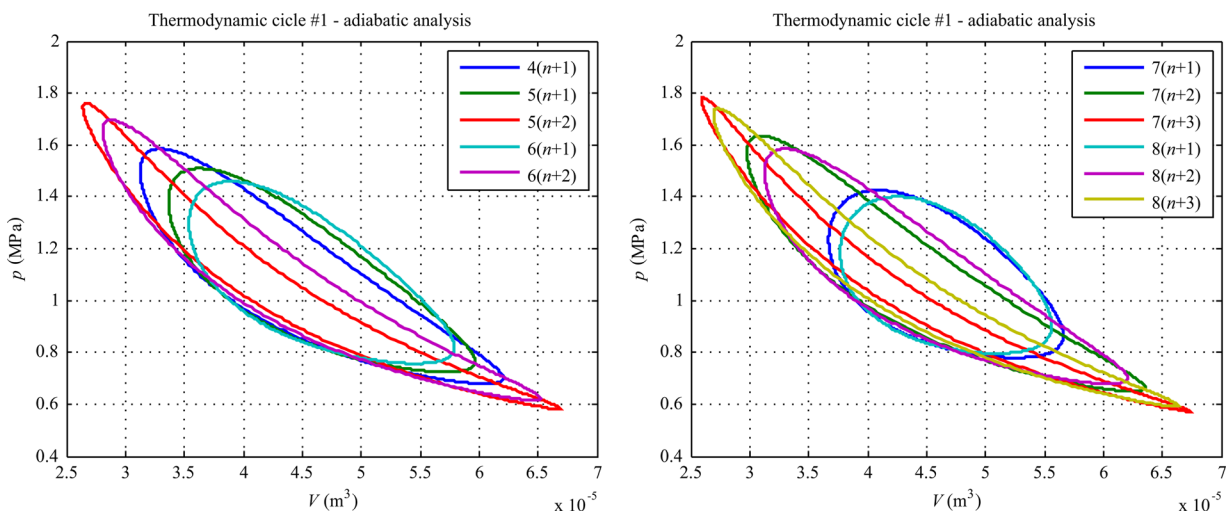

Fig. 14 *p–V* diagrams of the first thermodynamic cycle at steady state for different cylinder configurations

Table 2 Results of the simulations for several cylinder configurations

Config.	Δ (deg)	$\bar{P}$ (W)	$\bar{P}/N$ (W)	$\bar{M}$ (Nm)	$\Delta\bar{M}/\bar{M}$ (%)	$\eta = W/Q_e$ (%)
4 $(n+1)$	90	942	236	6,3	2,34	63.5
5 $(n+1)$	72	1152	230	7,7	0,22	64.5
5 $(n+2)$	144	647	129	4,3	1,00	59.0
6 $(n+1)$	60	1285	214	8,6	0,05	65.1
6 $(n+2)$	120	1181	197	7,9	0,12	61.8
7 $(n+1)$	~51	1375	196	9,2	0,02	65.5
7 $(n+2)$	~103	1581	226	10,5	0,07	62.8
7 $(n+3)$	~154	646	92	4,3	0,44	56.0
8 $(n+1)$	45	1439	180	9,6	0,02	65.8
8 $(n+2)$	90	1884	236	12,6	0,04	63.5
8 $(n+3)$	135	1265	158	8,4	0,16	60.4

points A and C differ only by the inertial forces of the wobble rod AC. The absolute values of the radial force of joints P and A as a function of the angular rotation of the electrical generator are shown in Figs. 15 and 16. In these figures, only the forces on the first cylinder of the mechanism at steady state are shown.

The radial force, the axial force and the torque for the revolute joint G of the rocker arm GD are shown in Fig. 17.

From Figs. 15–17 it is possible to highlight a reduction of the joint forces in the radial direction with respect to the four-cylinder configuration for configurations with a serial connection with the thermodynamic cycles, i.e., $k(n+1)$ with $k > 4$. For these configurations, the radial forces also do not cross the zero value, which means that the force acts only in one direction. This condition allows for possible problems because the internal joint backlash can be reduced.

Parametric Analysis

The effect of some geometrical parameters of the kinematic scheme on the total net power has also been investigated. In particular, only the significant parameters related to the slider-crank mechanism, which are the length $\overline{GD}$ of the rocker arm, the length $\overline{AC}$ of the wobble rod and the radial position $\overline{KP}$ of the pistons (see Fig. 5), have been considered in the analysis.

The results of this analysis are reported in Fig. 18 for the $5(n+1)$-cylinder configuration, where the mechanical power is plotted as a function of the aforementioned parameters. The analysis is performed by changing the distance $\overline{EH}$ of the scheme reported in Fig. 5 to maintain the same stroke indicated in Table 1. It is possible to observe from Fig. 18 that the maximum values of the power are located close to the boundaries of the parameter

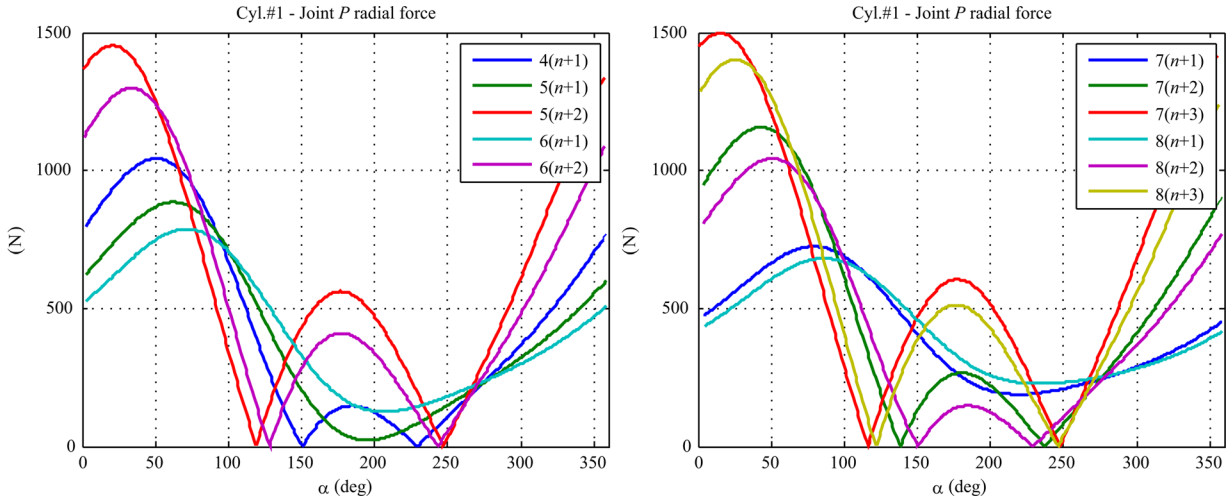

Fig. 15 Radial force at cylindrical joint *P*

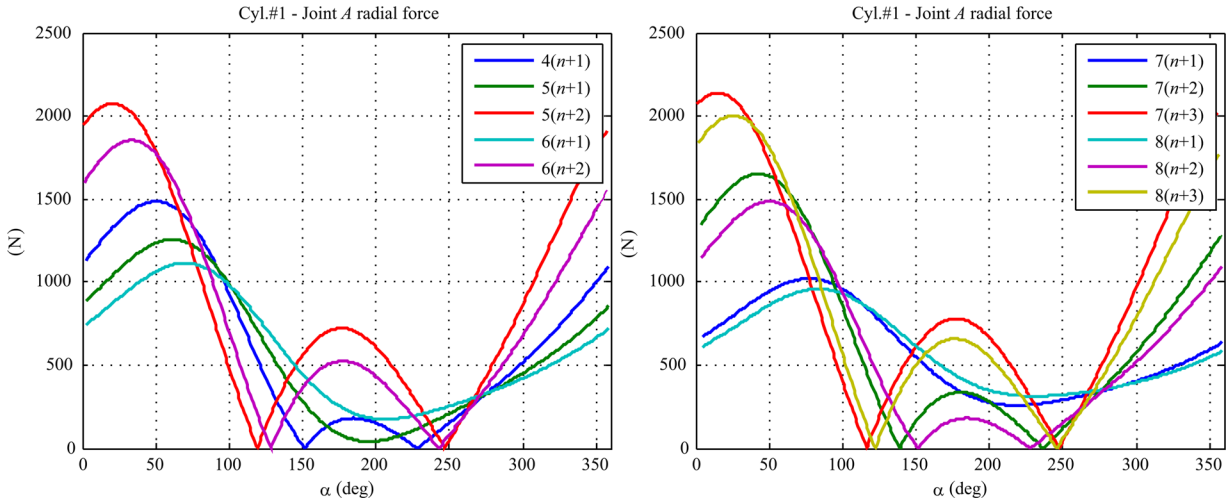

Fig. 16 Radial force at spherical joint *A*

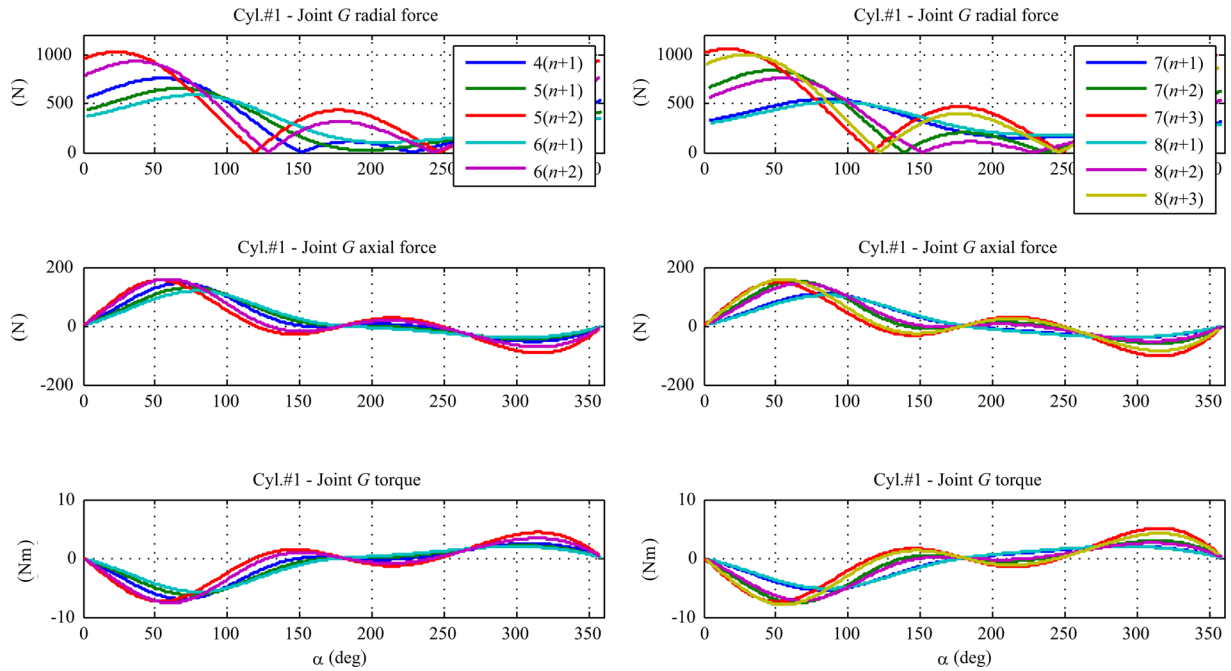

Fig. 17 Radial force, axial force, and torque at revolute joint *G*

analysis range. A section of Fig. 18, obtained for the condition $\overline{KP} = \overline{GD}$, is reported in Fig. 19. The condition $\overline{KP} = \overline{GD}$ is a reasonable geometrical condition for small oscillations of the connecting rod during a revolution of the crankshaft of the electrical generator shown in the scheme in Fig. 7. In Fig. 19, for a fixed value of the distance $\overline{KP} = \overline{GD}$, high values of the power are obtained simply by increasing the length $\overline{AC}$ of the connecting rod. Conversely, the maximum values for the power at the boundaries of the parameter analysis range in Fig. 18 correspond, in general, to the points of a singularity of the kinematic scheme or the dimensions of the elements not compatible with the design constraints given due to collisions or the physical dimensions of the rods.

The parametric analysis shows that an increase in power can also be obtained via small variations in the lengths of the elements of the kinematic scheme.

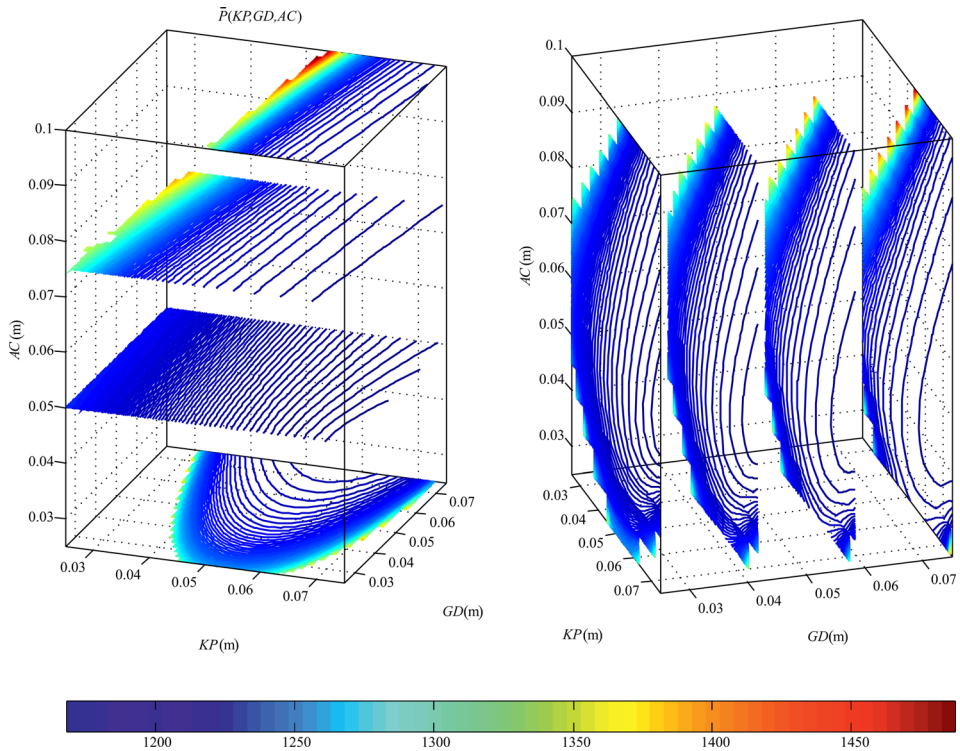

Fig. 18 Total net power (5 (n + 1)-cylinder configuration) as function of some geometrical parameters: length *GD* of the rocker arm, radial position *KP* of the piston, and length *AC* of the connecting rod

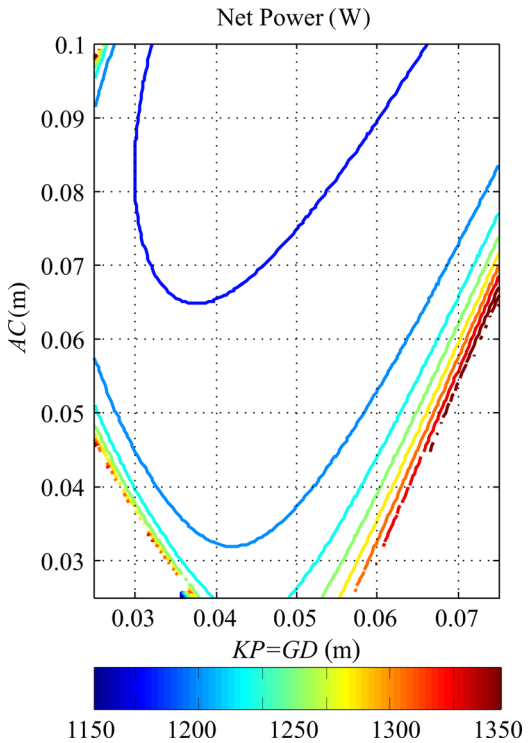

Fig. 19 Total net power for the 5 ($n+1$)-cylinder configuration as function of several geometrical parameters: length *GD* of the rocker arm equal to the radial position *KP* of the piston and length *AC* of the connecting rod

Conclusions

An investigation into different multicylinder configurations for a Stirling engine has been performed to study the effect of the increase in the number of cylinders on the total net power.

Models of both the thermodynamic cycle and the mechanical part of the engine have been described. The former considers adiabatic transformations in the compression and expansion spaces, whereas the latter includes all of the inertial properties. The simulations in the steady state have been performed via time integration of the equation sets. However, the analysis can be improved using a more detailed model of the heat exchangers, especially for the regenerator, and considering the frictional forces due to the seals between the pistons and the cylinders.

The effect of the friction in the pistons and joints depends on several design choices, such as the material, the preload of the seals, and the adoption of plain or rolling element bearings for the revolution joints in the mechanism. These effects need a deep investigation and can be evaluated in future experiments using the available prototype. In the same way, it will be possible to compare the power losses for the new planetary mechanism with respect to a commercial four-cylinder unit. It can be assumed that the power losses due to friction will increase with the number of cylinders due to the increase in the number of joints.

The analysis described in this paper was performed for several numbers of cylinders ranging from 4 to 8 and taking into account different connections of the thermodynamic cycles among the cylinder chambers.

An analysis of the number of cylinders has been performed by multiplying the basic kinematic scheme identified by the nth cylinder. The increase in the total mean power for high cylinder numbers is obvious. The highest specific mean power, given by the ratio between the total mean power and the cylinder number, is also found in the $4(n+1)$ configuration followed by the $5(n+1)$ and the $7(n+2)$ ones.

The reduction of the torque oscillations with respect to the torque mean values, given by configurations with high cylinder numbers, is more evident. The best configurations in terms of the increase of the mean torque and reduction of the torque oscillation at the output shaft are the $5(n+1)$ and the $7(n+2)$ configurations.

The analysis of the cylinder number shows that it is possible to increase the total net power with considerable benefits in terms of reducing the torque and speed oscillations. The authors have proposed a new design configuration that is able to increase the number of cylinders. Some of the design limitations of commercial four-cylinder engines, based on the wobble yoke mechanism, are solved using a planetary mechanism. The overall dimensions of the new engine in the eight-cylinder configuration with the planetary mechanism should the same as the commercial four-cylinder unit with the wobble yoke mechanism because it is possible to maintain the same radial positions of the cylinders for these two configurations. For example, the cost increase of a eight-cylinder unit compared with a four-cylinder one is mainly connected to the additional pistons and connecting rods. The cost of the planetary mechanism should be similar to that of a wobble yoke. In addition, the preliminary analysis of the effect of some kinematic parameters on the total mean power shows that it is possible to perform a considerable optimization of the system.

Nomenclature

$\overline{AC}$ = length of wobble rod AC
$\overline{BE}$ = axial distance between the center of the planetary mechanism and the center of slider-crank mechanism
$\overline{BG}$ = distance of the revolute joint of the rocker arm from the revolution axis of the electrical generator
c_p = specific heat of gas at constant pressure
c_v = specific heat of gas at constant volume
C_{gen} = torque of the electrical generator
d_s = stem diameter
D_p = piston diameter
$\overline{DP}$ = connecting rod length
$\overline{EH}$ = distance of the center of the planetary mechanism from the revolution axis of the electrical generator
$F_{comp,n}$ = fluid force on the lower surface of the piston (compression space)
$F_{exp,n}$ = fluid force on the upper surface of the piston (expansion space)
$\overline{GC}$ = distance of the joint of the wobble rod AC from the base joint of rocker arm GD
$\overline{GD}$ = length of rocker arm GD
$\overline{HA}$ = distance of the joint of the wobble rod AC from the center of the planetary disk
$j \in \{c,k,r,h,e\}$ = jth cell index: c = compression space, k = cooler, r = regenerator, h = heater, e = expansion space
J_I = mass moment of inertia of the idle gear
J_{DP} = mass moment of inertia of the connecting rod DP
J_{EH} = mass moment of inertia of the planetary carrier, including the inertia of the electrical generator
J_{GD} = mass moment of inertia of the rocker arm GD with respect to joint D
$\overline{KP}$ = radial position of the pistons
M = total mass of the gas
$\bar{M}$ = mean torque at the shaft of the electrical generator
m_I = Mass of the idle gear
m_j = mass of the fluid in the jth cell
m_p = mass of the piston and the cross-head
m_{AC} = mass of the wobble rod AC
m_{DP} = mass of the connecting rod DP

m_{GD} = mass of the rocker arm GD
m_{HA} = sum of the masses of the planetary gear and its shaft
$\dot{m}_{(j-1)\rightarrow j}$ = inlet mass flow in the jth cell
$\dot{m}_{j\rightarrow(j+1)}$ = outlet mass flow in the jth cell
N = number of cylinders, number of thermodynamic cycles
p = pressure of the fluid
$\bar{P}$ = total mean power
$p_{\mathrm{comp},n}$ = pressure of the fluid in the compression space of the nth thermodynamic cycle
$p_{\mathrm{exp},n}$ = pressure of the fluid in the expansion space of the $(n+1)$th thermodynamic cycle
$\dot{Q}_j$ = heat transfer into the jth cell
R = gas constant
T_j = temperature of the fluid in the jth cell
$T_{(j-1)\rightarrow j}$ = temperature of the inlet mass flow in the jth cell
$T_{j\rightarrow(j+1)}$ = temperature of the outlet mass flow in the jth cell
V_j = volume of the jth cell
V_{clc} = compression dead volume
V_{cle} = expansion dead volume
V_{swc} = compression swap volume
V_{swe} = expansion swap volume
W_j = work performed on the surroundings of the jth cell
$y_{p,n}, \dot{y}_{p,n}, \ddot{y}_{p,n}$ = displacement, velocity, and acceleration of the nth piston
Z_{E} = number of teeth of the sun gear
Z_{I} = number of teeth of the idle gear
$\alpha, \dot{\alpha}, \ddot{\alpha}$ = angular rotation, angular velocity, and angular acceleration of the shaft of the electrical generator
$\dot{\alpha}_0$ = nominal angular speed of the electrical generator
Δ = phase angle between two consecutive thermodynamic cycles
δ_n = geometrical phase between two consecutive cylinders
$\varepsilon_n, \dot{\varepsilon}_n, \ddot{\varepsilon}_n$ = angular rotation, angular velocity, and angular acceleration of the nth connecting rod DP
η = thermodynamic efficiency
$\phi_n, \dot{\phi}_n, \ddot{\phi}_n$ = angular rotation, angular velocity, and angular acceleration of the nth rocker arm

References

[1] Walker, G., 1973, *Stirling Cycle Machines*, Clarendon Press, Oxford, UK.
[2] Martini, W. R., 2004, *Stirling Engine Design Manual*, Martini Engineering Publication, University Press of the Pacific, Stockton, CA.
[3] Senft, J. R., 1993, *Ringbom Stirling Engines*, Oxford University Press, New York.
[4] Clucas, D. M., and Raine, J. K., 1994, "Development of a Hermetically Sealed Stirling Engine Battery Charger," Proc. Inst. Mech. Eng., Part C, **208**(6), pp. 357–366.
[5] Gopal, V. K., Duke, R., and Clucas, D., 2009, "Active Stirling Engine," TENCON IEEE Region 10 Conference, Singapore, Jan. 23–26, pp. 1–6.
[6] Kuhn, V., Klemeš, J., and Bulatov, I., 2008, "MicroCHP: Overview of Selected Technologies, Products and Field Test Results," Appl. Therm. Eng., **28**(16), pp. 2039–2048.
[7] Roselli, C., Sasso, M., Sibilio, S., and Tzscheutschler, P., 2011, "Experimental Analysis of Microcogenerators Based on Different Prime Movers," Energy Build., **43**(4), pp. 796–804.
[8] Karabulut, H., Yücesu, H. S., and Çınar, C., 2006, "Nodal Analysis of a Stirling Engine With Concentric Piston and Displacer," Renewable Energy, **31**(13), pp. 2188–2197.
[9] Karabulut, H., Çınar, C., Oztürk, E., and Yücesu, H. S., 2010, "Torque and Power Characteristics of a Helium Charged Stirling Engine With a Lever Controlled Displacer Driving Mechanism," Renewable Energy, **35**(1), pp. 138–143.
[10] Karabulut, H., Aksoy, F., and Oztürk, E., 2009, "Thermodynamic Analysis of a ß Type Stirling Engine With a Displacer Driving Mechanism by Means of a Lever," Renewable Energy, **34**(1), pp. 202–208.
[11] Eldesouki, E., 2009, "Performance of a Beta-Configuration Heat Engine Having a Regenerative Displacer," Renewable Energy, **34**(11), pp. 2404–2413.
[12] Karabulut, H., Çınar, C., Aksoy, F., and Yücesu, H. S., 2010, "Improved Stirling Engine Performance Through Displacer Surface Treatment," Int. J. Energy Res., **34**(3), pp. 275–283.
[13] Riofrio, J. A., Al-Dakkan, K., Hofacker, M. E., and Barth, E. J., 2008, "Control-Based Design of Free-Piston Stirling Engines," American Control Conference, Seattle, WA, June 11–13, pp. 1533–1538.
[14] Shendage, D. J., Kedare, S. B., and Bapat, S. L., 2011, "An Analysis of Beta Type Stirling Engine With Rhombic Drive Mechanism," Renewable Energy, **36**(1), pp. 289–297.
[15] Chatterton, S., Pennacchi, P., Vania, A., Ricci, R., and Ghisoni, A., 2012, "Design of a Stirling Machine in a Multi-Cylinder Configuration for Microcogeneration," ASME Paper No. GT2012-70096.
[16] Urieli, I., and Berchowitz, D. M., 1984, *Stirling Cycle Engine Analysis*, Adam Hilger Ltd., Bristol, UK.
[17] Kato, Y., and Baba, K., 2014, "Empirical Estimation of Regenerator Efficiency for a Low Temperature Differential Stirling Engine," Renewable Energy, **62**, pp. 285–292.